J Mater Sci (2012) 47:4370–4382
DOI 10.1007/s10853-012-6291-8

Processing and characterization of nanofibrillated cellulose/layered silicate systems

T. T. T. Ho · Y. S. Ko · T. Zimmermann · T. Geiger · W. Caseri

Received: 19 December 2011 / Accepted: 20 January 2012 / Published online: 3 February 2012

Abstract Recently, nanofibrillated cellulose with cationic functional groups was synthesized. This trimethylammonium-modified nanofibrillated cellulose (TMA-NFC) was applied in this study for the preparation of composites with various layered silicates. These belonged to the groups of montmorillonite, kaolin, talc, vermiculite, and mica. The respective composites were prepared by high-shear homogenization followed by filtration and hot-pressing. Data on crystal structures, chemical compositions, cation exchange capacity, specific surface area, density, and morphology of all clays and micas themselves as well as structure information of the corresponding composites have been collected. Possible microstructural features responsible for the composite appearances were tentatively identified. Principally, the interactions between TMA-NFC and the layered silicates were pronounced, due to electrostatic attraction of cationic cellulose fibrils and anionic silicate layers. This mutual interaction between TMA-NFC and layered silicate, however, was influenced not only by layered silicate properties but also by the composite preparation method, as discussed in this study.

T. T. T. Ho (✉) · T. Zimmermann
Applied Wood Materials, Empa, Swiss Federal Laboratories for Materials Science and Technology, Ueberlandstrasse 129, 8600 Duebendorf, Switzerland
e-mail: thuthao.ho@empa.ch

Y. S. Ko · W. Caseri
Institute for Polymer, ETH, Swiss Federal Institute of Technology, Wolfgang-Pauli-Str. 10, 8093 Zurich, Switzerland

T. Geiger
Functional Polymers, Empa, Swiss Federal Laboratories for Materials Science and Technology, Ueberlandstrasse 129, 8600 Duebendorf, Switzerland

Introduction

Clay minerals are natural products. They are used in a number of different commodities, such as building materials, ceramics, paper, paints, cosmetics, pharmaceutics, and geological products [1, 2]. In many applications, clay minerals are combined with polymers. When the clay particles are present in a highly delaminated state in the polymer matrix, the corresponding materials are attributed to the class of nanocomposites. The presence of clay can significantly improve the thermal stability [3], tensile properties [3], or barrier properties against gas and vapor transmissions [4, 5] of the polymer matrix.

Clay minerals belong to the class of layered silicates which is divided in various groups (e.g., kaolin, talc, mica, smectite, and vermiculite) that possess different structural characteristics. The structure of clays and micas is based on two types of layers: one tetrahedral sheet is bonded to one octahedral sheet in 1:1 layer structures, while in 2:1 layers, an octahedral sheet is sandwiched between two tetrahedral sheets [1, 2]. Kaolin consists of 1:1 dioctahedral layers. It is one of the most widely used pigments in paper industry and is well-known for providing gloss in coating applications. In talc structure, the interlayer space is free of ions, whereas in mica, it is occupied usually by potassium ions [6]. Muscovite and phlogopite are the most common micas due to their commercial importance (electrical industry). However, compared to other types of layered silicates, especially to smectite, there are relatively few reports on micas in composites [7], although mica platelets possess high aspect ratio and platy morphology. The interlayer space of smectite and vermiculite (2:1 layer structure) contains alkaline metal or alkaline-earth metal cations such as Na^+, K^+, Ca^{2+}, or Mg^{2+}, together with water molecules. Smectite and vermiculite silicate layers have smaller

negative layer charge than mica. Smectites represent an interesting group due to their high swelling capacity in water [1] that renders them suitable for many applications such as artificial geological barrier layer, absorbent in food industry or thickener [8]. A popular clay mineral of the smectite family is montmorillonite that is frequently used as a component in nanocomposites [9, 10].

Research on classical polymer/clay nanocomposites has predominantly been carried out using synthetic polymers as a matrix, for instance polyimides [4], polymethacrylates [11, 12], polyethylene [13], or polystyrene [11, 14]. However, the environmental impact of petroleum-based polymers, in particular in packaging industry, has stimulated efforts to replace these by sustainable, biodegradable and environmentally friendly polymers in composites with clays [15], for example, potato starch/montmorillonite [16] or poly(lactic acid) (PLA)/montmorillonite [17]. Cellulose fibers belong to the first choices when sustainable bio-materials are to be used [18], due to particular features such as renewability, biodegradability, non-abrasiveness, low density, and low cost [19, 20]. Systems of natural cellulose fibers and clays, however, have considerable drawbacks. Since natural cellulose fibers with diameters of 10–25 μm [21] provide very little specific surface area, the interface between clay and a matrix of cellulose fibers is small and their interactions, if possible at all, are limited. A reduction in fiber dimension, especially fiber diameter, would result in a much larger contact surface area with incorporated particles.

Consequently, nanofibrillated cellulose (NFC) is expected to be particularly suited as a matrix for composites with clays. The fiber diameters of NFC are below 100 nm and their lengths are in the micrometer range. NFC has been obtained from cellulose fibers by combinations of chemical, enzymatic, and mechanical treatments [22–24]. In fact, compared to native cellulose fibers, NFC possesses smaller fiber sizes (higher aspect ratio) and higher quantity of reactive surface –OH groups per mass unit of cellulose (due to larger specific surface area). NFC nanocomposites thus show a much higher grade of homogeneity, higher tensile strength and modulus, higher transparency [25–27] than composites of cellulose fibers. Recently, nanocomposites of polymers and NFC as a reinforcing component have been developed [28, 29], and few works on NFC/clay composites (so-called nanopaper) have been published lately [30, 31]. However, no study is available which deals with interactions between NFC and clay or mica.

Regarding interactions between NFC and clays or micas, it has to be considered in all systems that cellulose is negatively charged due to the presence of $-O^-$ and $-COO^-$ groups, and those groups basically repel the negatively charged silicate layers of clays and micas. This discrepancy leads to a lack of compatibility or adhesion at the interface between cellulose fibers and clay or mica platelets. However, optimum compatibility between cellulose and layered silicates is indispensable to address properties of ensuing composite materials like impermeability and high thermal stability [32, 33]. For these reasons, it is necessary to modify either the silicates or the cellulose fibers in order to improve the compatibility between the two components. Cationic groups at the cellulose surface are expected to be particularly suited to enhance the ionic interactions with the negatively charged silicate layers of clays and micas. Indeed, we have reported recently the preparation of cationized nanofibrillated cellulose (TMA-NFC) (see Fig. 1) for better ionic interaction with negatively charged montmorillonite clay layers [21]. However, in order to obtain homogeneous materials, the processing of the two component system is also pivotal.

Therefore, we investigated the processing and interaction of different kinds of layered silicates (clays and micas) with TMA-NFC in this study. For simplicity, TMA-NFC/layered silicate systems are denoted TMA-NFC/LS. Composites with well-characterized TMA-NFC [21] and layered silicates were produced by high-shear homogenization, filtration, and hot-press processes. In order to understand the interaction between cellulose fibrils and layered silicates, the morphology in both wet (suspension) and dry (film) systems was studied.

Experimental

Materials

TMA-NFC

Trimethylammonium-modified nanofibrillated cellulose (TMA-NFC) was prepared at a temperature of 97.5 °C as described earlier [21]. The available cationic groups in TMA-NFC were estimated based on the nitrogen content of trimethylammonium groups [21]. Cellulose pulp powder produced from oat straw (Jelucel OF300, Rosenberg, Germany) was used as starting raw material for the preparation of non-modified NFC and TMA-NFC.

Layered silicates

Thirteen different types of clays and micas were applied. Information about their suppliers as well as idealized formulae is displayed in Table 1.

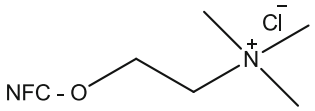

Fig. 1 Section of the structure of TMA-NFC illustrating the modifying unit

Table 1 Suppliers and suggested idealized formulae of layered silicates

Name	Supplier	Suggested formula	Reference
Montmorillonite EXM1246	Sud-Chemie AG (Germany)	$Si_4Al_{2-y}Mg_yO_{10}(OH)_2,yM^+\cdot nH_2O$	[1], $y = 0.6$
Kaolin Barrisurf HX	Imerys (France)	$Al_2Si_2O_5(OH)_4$	Supplier
Talc	Erne-Chemie Dallikon (Switzerland)	$Mg_3Si_4O_{10}(OH)_2$	[6]
Vermiculite grade 4	Virginia Vermiculite Limited (USA)	$Si_{4-x}Al_xMg_{3-y}M_y^{3+}O_{10}(OH)_2,((x-y)/2)Mg^{2+}$	[1], $x = 1.2$ and $y = 0.8$
Mica PW30	Minelco (UK)	$KMg_3Si_3AlO_{10}(OH)_2$	[6]
Mica R180	Microfine Minerals (UK)	$KAl_2Si_3AlO_{10}(OH)_2$	[6]
Micavor 20	Kaolins d'Arvor (France)	$KAl_2Si_3AlO_{10}(OH)_2$	[6]
Mica MU-M 2/1	Imerys (USA)	$KAl_2Si_3AlO_{10}(OH)_2$	[6]
Mica SYA 31R	Alberto Luisoni AG (Switzerland)	$KAl_2Si_3AlO_{10}(OH)_2$	[6]
Mica Sublime 325	Alberto Luisoni AG (Switzerland)	$KAl_2Si_3AlO_{10}(OH)_2$	[6]
Rona Flair Silk Mica	Merck KGaA (Germany)	$KAl_2Si_3AlO_{10}(OH)_2$	Supplier
Mica SX400	Minelco (UK)	$KAl_2Si_3AlO_{10}(OH)_2$	[6]
Mica R120	Minelco (UK)	$KAl_2Si_3AlO_{10}(OH)_2$	[6]

The formulae were taken from the literature or from declaration of the suppliers

Film processing

Homogenization, filtration, and hot-pressing

For the preparation of all films of TMA-NFC and different types of clay or mica (Table 1), a total mass of 4.41 g was always employed. Thus, in the case of a 1:1 ratio, in the first step, 2.205 g of TMA-NFC (scaled according to the dry content of TMA-NFC suspension) and 2.205 g of clay or mica were put into separate flasks. Water was then added to the TMA-NFC until the total mass of the suspension reached 500 g. After that, this TMA-NFC suspension was transferred to a high-pressure homogenizer (lab-scale microfluidizer type M-110Y, Microfluidics Corporation, USA, see [34]) and subsequently pumped at high velocities through fixed-geometry interaction chambers (Y or Z morphology) with diameters of 200 μm ($H30Z_{200\mu m}$) and 75 μm ($F20Y_{75\mu m}$). Water was also added to the clay or mica, until the concentration in water reached 5 wt%. While TMA-NFC suspension was pumping in the homogenizer, the clay or mica suspension was added at a rate of 5 mL/min. The applied pressure was always 1000 bar to generate the high-shear forces necessary to disintegrate and homogenize the NFC and layered silicate materials. The final suspension was left to pass through the chambers for 20 passes to homogenize the dispersion. Meanwhile, 200 mL of water had been added to the suspension, because NFC and clay or mica residues had to be collected from the flasks and the suspension container walls. The final concentration of TMA-NFC/LS in water was about 0.6 wt%.

The suspension was then transferred into a pressure filter, containing a twilled Dutch weave metal filter cloth (stainless steel AISI 316L, 325 × 2300 mesh) with pores size of 5 μm, supported by a more mechanical stable stainless steel mesh of larger pore size and a steel sheet with holes of 2.5-mm diameter. A pressure of 0.5 bar was applied in mounting steps until a stable but still wet film formed. The wet film together with the metal filter cloth was then encased in layers of blotting paper and one sheet of Teflon cloth placed directly on the wet film, in order to prevent the blotting paper from meshing with the sample. These layers were finally packed on a sheet of cotton and transferred into a vacuum bag (Fig. 5).

A pump was connected to the vacuum bag, and a vacuum (0.2 bar) was applied to remove water remnant, while the assembly was hot-pressed by a Suter LP420 presser (A. Suter AG Maschinenbau, Basel, Switzerland) at 105 °C and 150 bar. After 25 min, the heat was turned off and the film was left to cool down while still under pressure to reduce residual stress. The cooling process lasted for about 2–3 h.

Characterizations

TMA-NFC

Modified NFC was characterized by elemental analysis, methylene blue adsorption, X-ray powder diffraction, viscosity, and scanning electron microscopy (SEM) as reported earlier [21].

Clays, micas, and TMA-NFC/LS systems

Crystal structure Crystal structures were examined by powder X-ray diffraction (XRD) patterns of clay or mica particles pressed into pellet form taken by a PANalytical (Almelo, Netherland) X' Pert Pro diffractometer to identify

the type of the layered silicates. The diffractometer was equipped with a copper anode (Cu K_α radiation) operating at a wavelength $\lambda = 1.5418$ Å. Cu K_α radiations was generated at 45 kV and 40 mA and a Ge (111) monochromator. All XRD spectra were recorded in the interval of $2° < 2\theta < 80°$ with a step size of 0.033°. The reflected intensities were registered as functions of the diffraction angle 2θ.

Elemental composition The elemental composition of layered silicates was determined by wavelength-dispersive X-ray fluorescence (WD-XRF) spectroscopy. Prior to the WD-XRF measurements, the clay or mica samples were treated at 975 °C in an oven for 3 h to remove organic compounds. A thin polypropylene film was used to cover one end of a double open-ended sample holder. Treated powder samples were loaded into sample holders and exposed to the measurement. The XRF spectrometer used was a Philips PANalytical PW2400 (Netherland) gauge equipped with Rh X-ray tube with voltage and current of 60 kV and 40 mA, respectively. There were 3 setup detectors: flow counter (FC), sealed proportional counter (PC), and scintillation counter (SC).

Cation exchange capacity (CEC) The CEC was determined according to the literature [35]. A specific amount (ca. 150 mg for montmorillonite, 600 mg for vermiculite, 1 g for other kinds of layered silicates) of air-dried clay or mica samples was added to ca. 20 mL of ultrapure water and dispersed by ultrasonic treatment (20 kHz, 400 W, 3 min). The sonicated suspension was completely transferred into a 50-mL volumetric flask containing 5 mL of Cu complex solution (prepared with 0.02 mol of anhydrous Cu(II) sulfate and triethylene tetramine from FLUKA AG, Switzerland) and 1 mL of pH 7 buffer solution. The volumetric flask was filled up with ultrapure water to 50 mL, and the suspension was mixed well by turning the volumetric flask 30 times over head. After that, the sample was allowed to sediment. The supernatant suspension was then centrifuged in a microcentrifuge (Microcentaur, MSE, UK) at 13000 rpm for 20 min. The supernatant solution from the centrifugal tube was carefully pipetted into 1 cm measuring cell. This cell was inserted into a spectral photometer CADAS 100 (Dr Bruno LANGE, Germany) and the color intensity value, which was measured as absorbance (Abs), was recorded. With the help of the obtained values, the CEC was calculated based on the dry layered silicate weight, whereas the water content of the layered silicate samples was estimated from the mass obtained after drying clays and micas at 105 °C until constant weight.

The CEC was calculated from the quantity of Cu^{2+} ions that did not adsorb on the silicate by cation exchange, that is, from the concentration of the Cu^{2+} ions in the supernatant solution after sedimentation of the clay or mica particles. This concentration was obtained by measuring the absorbance of a supernatant solution, in accordance with Beer–Lambert's law. The absorbance of a solution without clay or mica was also determined as a reference. The following formula was used for the calculation of the CEC [35]:

$$\mathrm{CEC} = \frac{((\mathrm{Abs}_{\mathrm{ref}} - \mathrm{Abs}_{\mathrm{LS}})/\mathrm{Abs}_{\mathrm{ref}}) \times 0.02 \times 10 \times 1000 \times 100}{m_{\mathrm{LS}}} \quad (1)$$

where CEC is the cation exchange capacity in milliequivalents (or millimol) per 100 g layered silicate; $\mathrm{Abs}_{\mathrm{ref}}$ is the initial absorbance of Cu^{2+} in a reference sample (absence of layered silicate); $\mathrm{Abs}_{\mathrm{LS}}$ is the absorbance of the supernatant solution after sedimentation of layered silicate; m_{LS} is the mass of the dry layered silicate sample in mg.

The factor 0.02 refers to the initial molar concentration of Cu^{2+} in solution.

The factor 10 corresponds to the dilution: 5 mL of Cu^{2+} solution was diluted to 50 mL in the cation exchange reaction with layered silicate.

The factor 1000 results from the conversion of mol to millimol, which is the common quantity indicated in CEC values.

The factor 100 results from the conversion of g to 100 g of layered silicate, which is the common quantity indicated in CEC values.

Specific surface area The specific surface area of all clay and mica samples was measured by nitrogen adsorption at −196 °C (BET method) in the relative pressure range $p/p_0 = 0.05$–0.3 with a volumetric sorption analyzer (Autosorb 1MP, Quantachrome Instruments, USA). The standard Brunnauer–Emmett–Teller (BET) method was used to calculate the specific surface area. Prior to the measurements, the powder samples of clay or mica were filled into the sample cell, degassed at 150 °C overnight, and purged with helium. The amount of layered silicate samples used was noted by weighing the empty sample cells and the cells after degassing.

Density The density of all layered silicate samples was measured with an AccuPyc 1330 Helium Pycnometer (Micromeritics Instrument Corporation, USA). Ca. 2 g of the powdered samples was loaded into an aluminum pan that was placed in a chamber of defined volume, and the air was subsequently exchanged by helium. The pressures observed upon filling the sample chamber and the subsequent discharge into a second empty chamber allowed calculation of the sample volume. The density was determined as the average value of 10 runs.

Morphology of layered silicates and TMA-NFC/LS composites The morphology of clays, micas, and TMA-NFC/LS samples was studied by SEM. SEM images were taken with a FEI Nova NanoSEM 230 instrument (FEI, Hillsboro, Oregon, USA). The clay or mica powder samples were prepared by sprinkling small amounts of as-received powder on carbon adhesive tape. In the case of NFC/LS suspensions, SEM pictures were taken after the homogenization step. Such samples were prepared from a diluted 0.05 wt% suspension of which 2–3 drops were placed on a sample holder. Samples of NFC/LS composite films were prepared by fracturing the films in liquid nitrogen. The pieces thus obtained were then fixed on a sample holder with the fracture area facing upwards. All samples were sputter coated directly with a platinum layer of about 8 nm (BAL-TEC MED 020 Modular High Vacuum Coating Systems, BAL-TEC AG, Liechtenstein) in Ar as a carrier gas at 5×10^{-2} mbar. SEM images were recorded with an accelerating voltage of 5 kV and a working distance of 5 mm. In order to understand in details the morphologies and dimensions of montmorillonite EXM1246 and mica R120, as-received powder samples of these layered silicates were dispersed in deionized water and stirred overnight. The obtained suspensions were prepared for SEM investigations as described above for NFC/LS suspension systems.

Results and discussion

Clay and mica characteristics

Crystal structure

Figure 2 shows XRD patterns of clays including montmorillonite, kaolin, talc, vermiculite, and two kinds of mica, phlogopite and muscovite.

According to literature [36], the interplanar spacing $d(001)$ of montmorillonite, kaolin, talc, vermiculite, and mica (both muscovite and phlogopite) amounts to around 11.8, 7.2, 9.35, 14.3, and 10 Å, respectively. The diffraction angle 2θ can be recorded and converted to the interplanar spacing d based on Bragg's equation, $n^*\lambda = 2^*d^*\sin\theta$ [36]. The XRD patterns in Fig. 2 show peaks at 2θ of 7.4, 12.3, 9.4, 6.2, and 8.8° for montmorillonite, kaolin, talc, vermiculite, and mica, respectively. These angles agree with the above mentioned interplanar spacings $d(001)$. The findings imply that the respective layered silicates are at least the main component in the used samples. Of course, certain structural defects have to be expected since all used minerals are natural products.

The absence of sharp peaks in the montmorillonite pattern should be noted. The broad peaks in XRD patterns

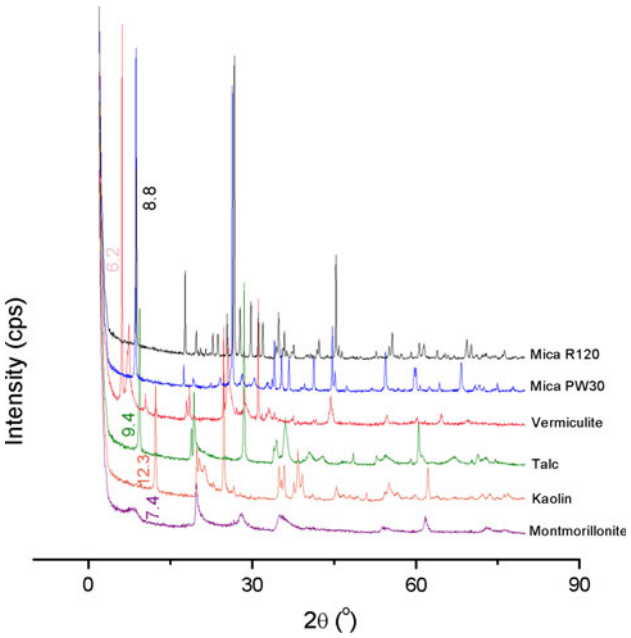

Fig. 2 XRD spectra of montmorillonite, kaolin, talc, vermiculite, and 2 kinds of mica: phlogopite (PW30) and muscovite (R120). The XRD spectra of other grades of muscovite are similar to that of mica R120 and are, therefore, not shown

of this type of clay could indicate that the crystallites are small or that crystal defects are considerable. Other layered silicates like kaolin, talc, vermiculite, and mica indicate well-crystallized structures through sharper peaks. In fact, SEM investigations (see below) disclose that the particle size of montmorillonite is smaller (compare Fig. 4) than in the other layered silicates, while the deviations of the elemental contents from the idealized composition of the montmorillonite are in the range of the other layered silicates investigated here (see below). Therefore, we attribute the broadness of the XRD pattern of montmorillonite to a small crystallite size rather than an uncommon deviation in the chemical composition.

Chemical composition

In order to evaluate the purity of the supplied samples, WD-XRF measurements were conducted to analyze the chemical composition. Table 2 shows the obtained values for Na, Mg, Al, Si, K, Ca, and Fe, which were then compared to the compositions derived from idealized formulae. Other elements, for instance Ti or Cl, were found only in minor quantities and are, therefore, not presented in Table 2.

Since clays and micas are natural products, variations of the chemical compositions can occur, which was actually evident from the analyses. Fe, Ca, Mg, and Na were frequently present as impurities. This leads to a difference in

Table 2 Chemical composition (in weight percent) of clays and micas determined by WD-XRF spectroscopy

Name	Na	Mg	Al	Si	K	Ca	Fe
Montmorillonite EXM1246	3.90 (3.70)	3.70 (3.92)	10.00 (10.14)	30.00 (30.16)	0.37	1.50	2.90
Kaolin Barrisurf HX	0.07		24.01 (20.90)	24.39 (21.76)	0.45	0.01	0.45
Talc		19.79 (19.23)	0.22	30.14 (29.62)		0.07	1.46
Vermiculite grade 4		12.24 (14.55)	7.78 (7.91)	18.76 (19.22)	3.59	1.82	10.17 (10.92)
Mica PW30		15.23 (17.48)	5.63 (6.47)	19.67 (20.19)	8.75 (9.37)	0.46	7.17
Mica R180	0.63	0.49	18.19 (20.32)	22.12 (21.16)	8.88 (9.82)	0.08	3.57
Micavor 20	0.18	0.47	18.25 (20.32)	23.96 (21.16)	8.02 (9.82)	<0.01	1.85
Mica MU-M 2/1	0.24	0.48	17.76 (20.32)	24.65 (21.16)	7.79 (9.82)	0.01	1.49
Mica SYA 31R	0.54	0.73	18.91 (20.32)	22.20 (21.16)	8.91 (9.82)	0.03	1.92
Mica Sublime 325	0.45	0.48	18.16 (20.32)	22.07 (21.16)	9.07 (9.82)	0.05	3.44
Rona Flair Silk Mica	0.61	0.27	20.25 (20.32)	22.15 (21.16)	8.75 (9.82)		1.34
Mica SX400	0.42	0.38	17.80 (20.32)	24.73 (21.16)	7.28 (9.82)	0.08	1.83
Mica R120	0.36	0.42	18.03 (20.32)	21.63 (21.16)	9.20 (9.82)	0.02	4.30

In round brackets values of chemical composition of the respective layered silicates calculated from their suggested formulae (see Table 1)

the quantity of the basic metal cations relative to their ideal compositions.

The chemical composition of mica PW30 fitted to phlogopite formula, while the other micas had compositions in agreement with muscovite. Notably, we observed 7.2% of Fe in phlogopite (PW30). Therefore, the dark color of PW30 can be explained by the presence of this element. This was also the case for vermiculite, where the Fe content was 10.2%. Observably, there were similarities in the content of the impurities Fe regarding mica R180, mica Sublime 325, and mica R120.

Cation exchange capacity, specific surface area, density, and morphology

Table 3 displays the CEC, specific surface area, and density values of clays and micas. Densities were measured to allow the calculation of volume fractions from mass fractions in composites. The densities were between 2600 and 3000 kg/m^3, that is, in a common range for clays and micas. Most of the mica types have slightly higher densities compared to the other clay types. This might cause higher compactness of the composites when including these layered silicates as fillers.

The CEC of the layered silicates was measured in aqueous suspension, while the specific surface area was determined by the BET method using layered silicates in the solid state. Note that the specific surface area in aqueous dispersion would be considerably higher than detected by the BET method, as a part of the particles are expected to pack so densely upon drying that the nitrogen molecules employed in the BET method will typically not have access to all the particle interfaces. Thus, the values determined here by the BET method are considered as the minimum specific surface areas with regard to the dispersed state in aqueous suspension.

Montmorillonite and vermiculite had, respectively, the highest and the second highest CEC and specific surface areas, as shown in Table 3. The CEC of montmorillonite was 102 mEq/100 g of clay (compared to 106 mEq/100 g indicated by the supplier), vermiculite followed with a value of 23 mEq/100 g. The other clays and micas exhibited very low values of between 0.5 and 3 mEq/100 g. The specific surface area for montmorillonite was 43 m^2/g followed by vermiculite with 15 m^2/g; the values of the other layered silicates were in the range of 2.3–9.5 m^2/g. Among all mica types, PW30 and R120 showed the highest specific surface areas in dry state.

Having the highest values of CEC as well as specific surface area, montmorillonite and vermiculite are expected to show highest ionic interactions with cationic fibrils compared to other layered silicates. CEC value of vermiculite is much lower than literature value; however, the used copper complex method is much simple and rapid compared to ammonium acetate method [37].

Remarkably, kaolin and talc are expected from the ideal structures to possess almost neutral layer charges (around 0 charge per $[O_{10}(OH)_2]$ formula unit); in contrast to micas (layer charges of around 1 charge per $[O_{10}(OH)_2]$ formula unit) [36]. In general, the distribution of the exchange cations in the interlayer space should be connected with the charges on the silicate sheet which they neutralize. The layers of mica, however, are firmly held to each other by the potassium interlayer cations. Normally, the interlayer cations of mica are not exchangeable. Similarly, vermiculite has interlayer cations that are only partial exchangeable with copper ions. This results in low CEC values of micas and lower CEC value of vermiculite. The existence of

Table 3 Cation exchange capacity, specific surface area, and density values of clays and micas

Name	CEC (mEq/100 g)	Specific surface area (m^2/g)	Density (kg/m^3)
Montmorillonite EXM1246	101.50	42.99	2681
Kaolin Barrisurf HX	2.53	9.54	2626
Talc	2.60	8.71	2803
Vermiculite grade 4	23.45	14.50	2782
Mica PW30	2.79	7.88	3005
Mica R180	1.33	4.60	2954
Micavor 20	1.27	5.31	2824
Mica MU-M 2/1	1.48	5.44	2861
Mica SYA 31R	1.03	5.62	2921
Mica Sublime 325	0.99	3.62	3000
Rona Flair Silk Mica	0.44	2.29	2936
Mica SX400	2.92	5.99	2814
Mica R120	1.67	7.19	2928

impurities, such as Na^+, K^+, Mg^{2+}, Ca^{2+}, etc. ions, should also be taken into account when evaluating CEC of layered silicates [38, 39].

As a matter of fact, the potential interaction of layered silicates with TMA-NFC is expected to increase with increasing number of exchangeable cations per unit surface area. This number, however, cannot be determined reliably from the specific surface areas obtained with the BET method and the CEC because the former does not represent the specific surface area in suspension (see above). In addition, it is possible that high-shear force of homogenization process could help to split the layers and, therefore, to increase the ionic interactions of negatively charged clay or mica layers with positively charged cellulose fibrils.

Most of the investigations are conducted in dry state (powder) of clay or mica, and therefore, the behavior of clay or mica can differ in those systems from that in the wet state (suspension).

SEM images of as-received materials (Fig. 3) provide information on the morphology and, roughly, the size of the different clays and mica particles. The surfaces of the montmorillonite particles are rougher than those of other clays and micas. From Fig. 3, it is clearly visible that as-received layered silicates are in fact the agglomerates of smaller particles. The high roughness and irregular shape of montmorillonite particles, containing pits and holes, may indicate that they are composed of particularly small particles not resolved in the image (Fig. 3a). This is in fact confirmed upon the dispersion of the particles in water (see Fig. 4). Comparing the layered silicate particle sizes, it is obvious that the largest montmorillonite platelets are much smaller than the largest mica platelets. Further, also from images of layered silicate suspensions shown in Fig. 4, montmorillonite has irregular flake-like shape, whereas mica particle has plate-like shape and smoother surface. It was also noted from the previous section that the broad peaks in the montmorillonite XRD pattern (Fig. 2) are in agreement with the small crystallite sizes in montmorillonite. When the clay anionic platelets are flexible (in particular montmorillonite), they can cover the cationic NFC fibrils because of good enough contacts.

Processing and film preparation

Up to now, there was no previously successful study on interactions between NFC and layered silicates, especially when employing cationic modified NFC. Furthermore, montmorillonite was the only clay applied in nanopaper [30, 31] even though there is large variety of clays or micas in nature.

The TMA-NFC/LS film preparation process is summarized in Fig. 5. To the best of our knowledge, high-shear homogenization method has not yet been used in NFC/clay composite processing. Under the high-shearing forces, the layered silicates might be disintegrated into thinner layers. In addition, these layers were broken into smaller particles that had diameters less than 75 μm in order to pass through the 75 μm chamber.

Regarding film preparation time, solvent casting generally required much time, for example, from 5 days [40] to 1 month at room temperature [41]. In addition, the advantage of a pressure filter compared with the traditional vacuum filter used in other studies [42] was a high flow rate of filtrates through the sieve (twilled Dutch weave metal filter cloth), which resulted in short filtration time, that is, in the range of 20–90 min. In addition, by application of metal filter cloth instead of filter paper, we could easily separate the dried NFC/LS film after hot-pressing from the filter cloth. In respect of hot-pressing conditions, 105 °C and 150 bar and a vacuum bag were applied in order to achieve the dried and well-packed films.

Morphology and structure of TMA-NFC/layered silicate systems

SEM images were used to study the morphology and structure of NFC/LS systems. Such composites with TMA-NFC were prepared and investigated with 13 layered silicates, and some representative examples are displayed in Figs. 6 and 7. The quantity of the clays and micas was always 50 wt% with respect to NFC.

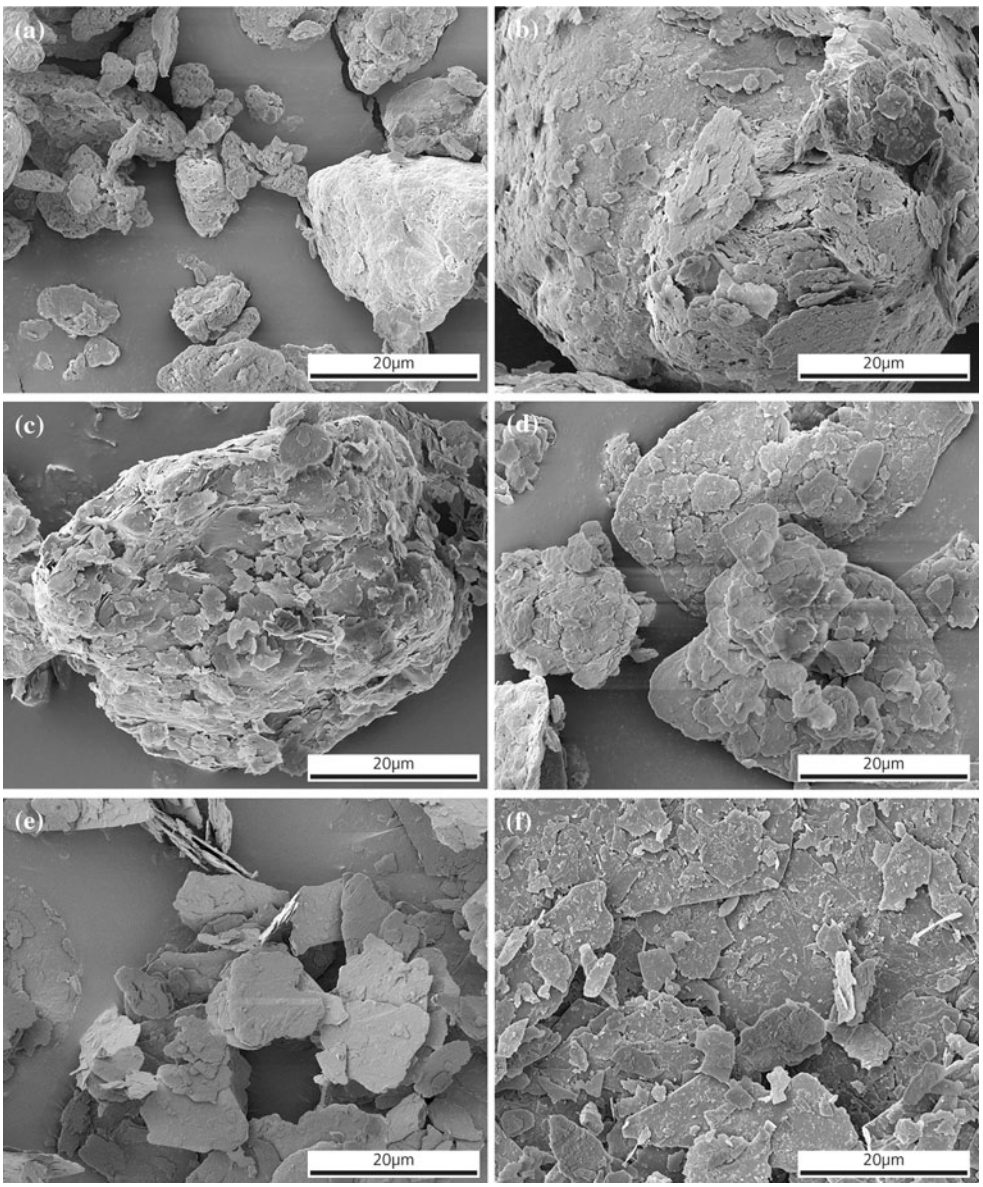

Fig. 3 SEM images of as-received clay and mica powders. **a** montmorillonite EXM1246, **b** kaolin Barrisurf HX, **c** talc, **d** vermiculite grade 4, **e** mica PW30, **f** mica R120

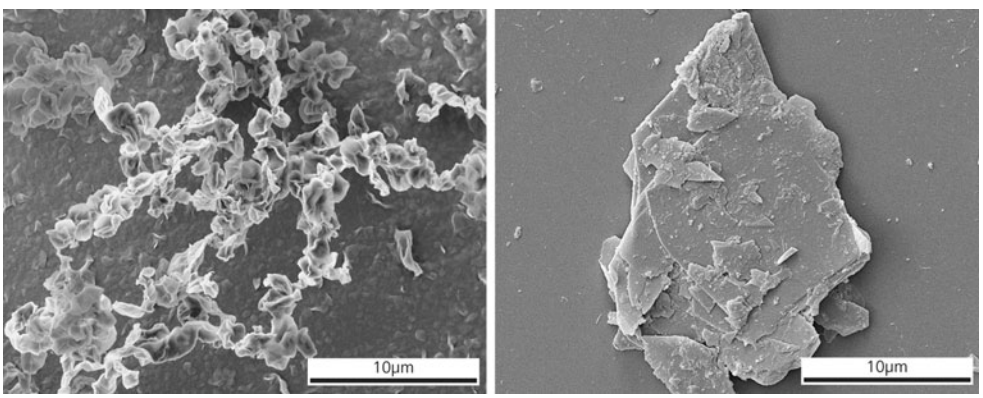

Fig. 4 SEM images of dried suspensions of montmorillonite EXM1246 (*left*) and mica R120 (*right*)

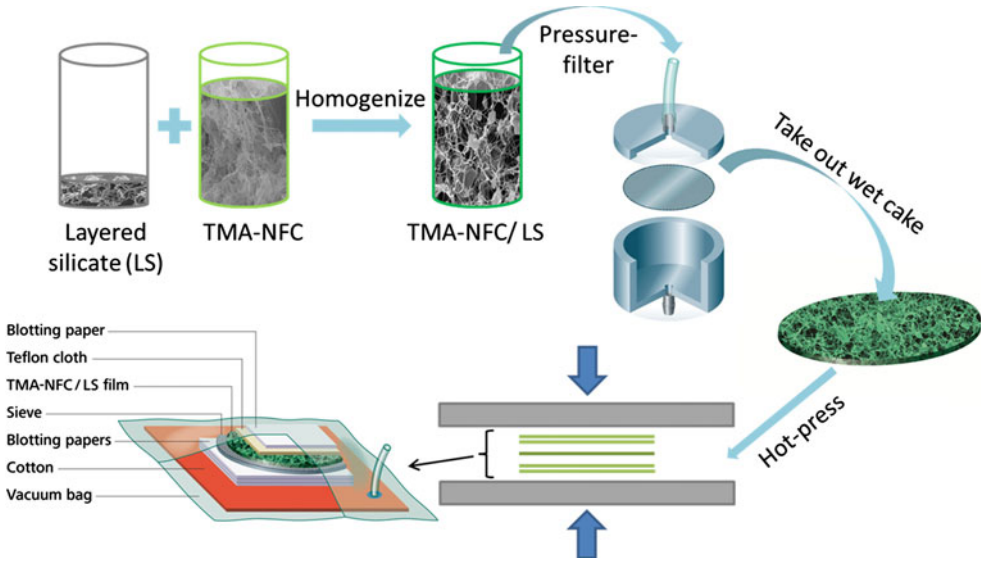

Fig. 5 NFC/LS film preparation scheme. At the end of the scheme, the layer structure of the vacuum bag assembly is displayed

Suspensions

Figure 6 shows SEM images of dried suspensions of TMA-NFC/LS (see Experimental section) typical for each group of layered silicates. For comparison, SEM images of non-modified NFC and mica R120 are shown in Fig. 6f. It is obvious that the mica platelets are not well distributed in the non-modified NFC network. Remarkably, although the mica concentration is 50 wt%, only a few, randomly distributed mica platelets are visible in the NFC network. This indicates that there is no significant interaction of silicate platelets and non-modified NFC fibrils, probably as a result of electrostatic repulsion between the negatively charged silicate layers and the negatively charged surfaces of the NFC fibrils.

In contrast, for all systems of cationic NFC and anionic layered charged clays or micas, the SEM images generally indicate good adhesion of clay or mica surfaces to TMA-NFC fibrils, as indicated by the good distribution of the layered silicates in the NFC network. This is most likely due to ion exchange of ammonium groups in TMA-NFC and the resulting electrostatic attraction with the negatively charged surfaces of the silicate layers. Notably, homogeneous distribution of clay or mica throughout the TMA-NFC network was achieved, even at a very high clay or mica concentration of 50 wt%, as used in this study. Normally, the percentage of clay used as filler in polymer/clay nanocomposites is less than 5 wt% [10, 43].

In the suspensions of TMA-NFC and kaolin or talc (Fig. 6b, c), many large stacks of clays that are not well distributed in the NFC networks are visible. Let us remind that kaolin and talc are composed of octahedral sheets with almost no charge on their layer surface. This renders kaolin or talc platelets less susceptible to ionic interactions with cationic TMA-NFC fibrils.

Interestingly, the tissue-like shaped platelets of montmorillonite, which are bent and folded and do not have a specific alignment (see above), are flexible enough to cover the TMA-NFC fibrils and thus forming a coherent composite network. However, they do not cover the voids between the NFC fibrils (compare Fig. 6a). Although a dense and even structure was formed from TMA-NFC and montmorillonite, the irregular shapes of montmorillonite are assumed to limit the formation of close or sealed contacts between trims or boundaries of clay flakes. On the contrary, the relatively flat and smooth vermiculite or mica platelets are supposed to be more suitable to seal voids or gaps in the composite systems. In fact, the platelets of vermiculite or mica show strong interactions with TMA-NFC and are, therefore, attached to fibrils in NFC networks (see insets from Fig. 6d, e). It is also visible from Figs. 6d and e that they are able to cover the voids. Note that all the SEM images were taken from highly diluted suspensions, that is, 0.05 wt%.

When considering a specific area of clay or mica surface in TMA-NFC/LS suspension, for example, 4 μm^2, derived from high magnification SEM images, it was possible to estimate the number of contacts between fibrils and layered silicates. Since the TMA-NFC fibrils were coved by montmorillonite flakes (Fig. 6a), this rough counting was only applied for kaolin, talc, vermiculite, or mica systems. Very few contacts (2–6) were seen in suspensions of kaolin, talc with TMA-NFC or mica with non-modified NFC (Fig. 6b, c, f), whereas 35 till 45 contacts were observed in TMA-NFC/vermiculite and TMA-NFC/mica R120, respectively (Fig. 6d, e).

It should be noted that flocculation was observed when clay minerals were added to TMA-NFC suspensions. This flocculation problem was diminished after passing the mixtures through high-pressure homogenizer. Flocculation

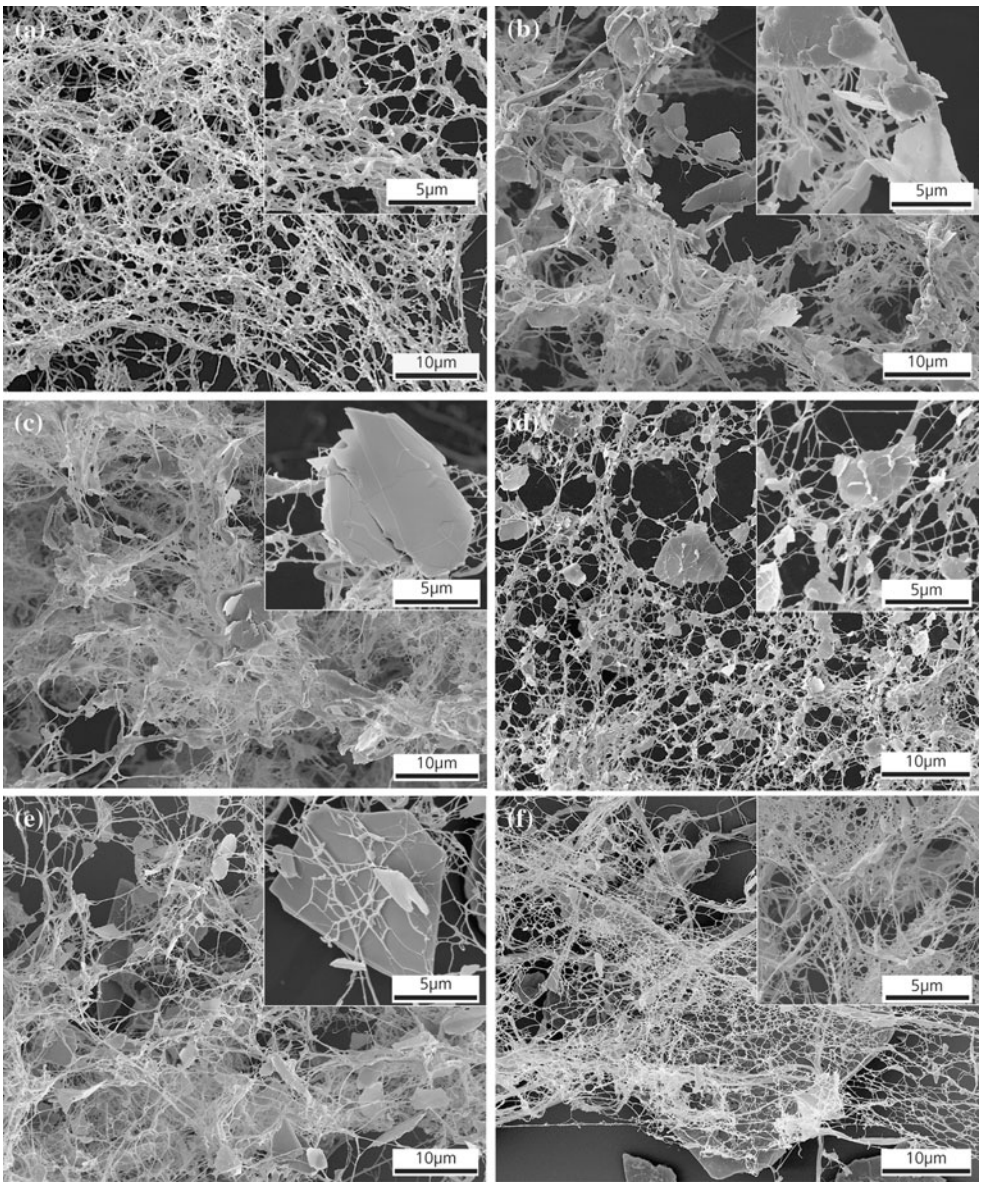

Fig. 6 SEM images of dried suspensions of NFC/layered silicates diluted to 0.05 wt% followed by evaporation of the water. In all systems, the fraction of clay or mica is 50 wt% with respect to NFC. **a** TMA-NFC/montmorillonite, **b** TMA-NFC/kaolin, **c** TMA-NFC/talc, **d** TMA-NFC/vermiculite, **e** TMA-NFC/mica R120, **f** non-modified NFC/mica R120. *Insets* images at higher magnification for further observations of interactions between cellulose fibrils and silicate layers

is probably caused by ionic attraction between cationic fibrils and anionic silicate layers and is, therefore, regarded as a qualitative indication of interactions between TMA-NFC and layered silicates.

Composites

The TMA-NFC/LS composite films were prepared as described in the Experimental section and as illustrated in Fig. 5.

Figure 7 presents SEM images of cross-sections of freeze-fractured composite films from the same TMA-NFC/LS systems described previously. Remarkably, all the NFC/LS composite films show a layered structure with parallel clay or mica platelets oriented in-plane with the cellulose. These layers are aligned. For comparison, a SEM image of non-modified NFC and mica R120 is shown in Fig. 7f.

The structure of the TMA-NFC/montmorillonite film seems to be slightly denser compared to the other composites, although the applied layered silicate concentrations were the same for all films (50 wt%). Again, it is evident that the montmorillonite particles are finer than the other layered silicate particles as the former cannot really be

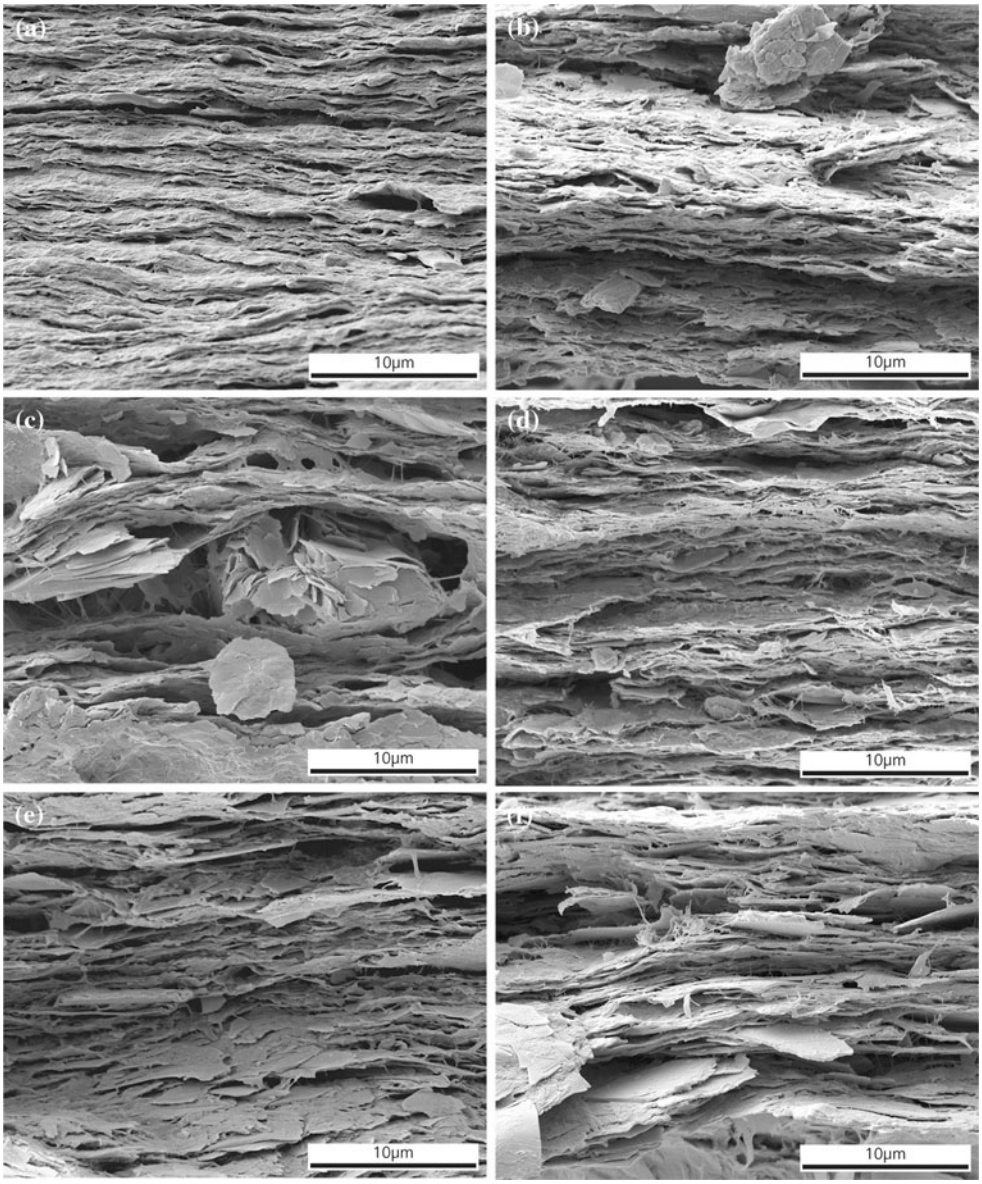

Fig. 7 SEM images of TMA-NFC/layered silicate film cross-sections of freeze-fractured surfaces. In all composites, the layered silicate concentration is 50 wt%. **a** TMA-NFC/montmorillonite, **b** TMA-NFC/kaolin, **c** TMA-NFC/talc, **d** TMA-NFC/vermiculite, **e** TMA-NFC/mica R120, **f** non-modified NFC/mica R120

distinguished in the respective SEM image (Fig. 7a). Mica and vermiculite composites (Fig. 7d, e) show clear and thin layer structures where silicate platelets can be easily recognized. These layers do not interpenetrate each other opposed to layers of montmorillonite composites. Interestingly, micas of all grades have interacted with TMA-NFC similarly to vermiculite with TMA-NFC, but with slightly higher level or denser contacts. If only based on SEM investigations, the differences between micas regarding the interactions with TMA-NFC cannot be clearly differentiated. Further studies on platelet dimensions and aspect ratio of micas are necessary to make substantiated claims. Platelet dimensions of clays and micas before (as-received) and after (in combination with TMA-NFC) homogenization, however, can be qualitatively compared from Figs. 3, 6. The starting materials have diameters of 2–120 μm (Fig. 3), while the homogenized materials have dimensions in the range of ca. 0.25–10 μm (Fig. 6). Many thick clay or mica stack aggregations are detectable in the composite films of kaolin or talc with TMA-NFC, or mica R120 with non-modified NFC (Fig. 7b, c, f). These findings are in accordance with those described in previous section, derived from the images shown in Fig. 6.

Thus, the oriented multilayer structure has been achieved by high-shear homogenization, filtration, and

hot-pressing processes, which up to now has been only mentioned when using the more time-consuming layer-by-layer deposition techniques [44, 45]. There are two important factors like applied shearing forces and cationization of cellulose fibrils when discussing interactions between cellulose fibrils and clay or mica layers. The applied shearing forces during the high-pressure homogenization process caused delamination of layered silicate particles into thinner stacks or lamellae which were subsequently attached to the positively charged fibril surfaces due to ionic interactions or cationic exchange mechanisms. In other words, both cationization of cellulose fibrils and high-shear homogenization may be optimal to initiate good interactions between TMA-NFC and layered silicates.

However, there were still minor silicate layer stacks in the system of cationic NFC and anionic silicate layers; that is, the clays were not completely delaminated into single silicate layers and not fully dispersed into the NFC network (complete delamination is not expected for the micas due to the larger attraction of the silicate layers by the interlayer cations, see above).

Conclusions

The study has given an overview of ionic interactions between NFC and different families of layered silicates. Thirteen types of layered silicates that belong to smectite, kaolin, talc, vermiculite, and mica groups were used to produce composites with cationic nanofibrillated cellulose (TMA-NFC) using a process of high-shear homogenization, filtration, and hot-pressing. Montmorillonite and vermiculite had higher cation exchange capacities and specific surface areas compared to other layered silicates. Montmorillonite had smaller crystallite size, smaller platelet dimensions, and rougher platelet surface. Thus, montmorillonite clay interacts differently with cationic fibrils compared to vermiculite, mica, kaolin, and talc. While montmorillonite clay layers covered cationic cellulose fibrils, vermiculite and mica platelets were rather attached on TMA-NFC networks, as indicated by respective suspensions after drying. There were no significant interactions between kaolin or talc and TMA-NFC. This resulted in the visible larger stacks of kaolin and talc in the systems with TMA-NFC. Experiments with non-modified NFC were also performed for comparison. The interactions of modified NFC and non-modified NFC with layered silicates also showed dissimilarities: There were no significant interactions between non-modified NFC and mica, in contrast to systems with the cationic TMA-NFC. This was also evident in parallel oriented multilayered structures of hot-pressed composite films of NFC and layered silicates as montmorillonite formed particularly dense composite structures with TMA-NFC, while other TMA-NFC/LS composite films had clearer and more distinguishable layered structures.

These findings were explained based on different interaction types, that is, electrostatic attraction or repulsion in NFC/LS systems. In any case, the cationic functional trimethylammonium groups of NFC are essential in this study for compatibility of NFC and layered silicates. In addition, the NFC/LS composite processing method, especially with the application of high-shear homogenization, possibly impacted the distribution of layered silicates in NFC networks.

Systems of montmorillonite clay and TMA-NFC displayed the best interaction level, where the clay flakes covered the cationic cellulose fibrils and formed a dense structure. Vermiculite and mica, due to the flatly morphologies, however, exhibited a high tendency of voids coverage.

The mechanical and barrier properties of NFC-LS composites will be evaluated in the next steps to understand further the interactions between these elements as well as to draw further possible applications for NFC/layered silicate composites.

Acknowledgements The authors kindly acknowledge the Commission for Technology and Innovation (CTI) for financial support. The authors particularly thank Anja Huch and Esther Strub for performing SEM; Urs Gfeller and Oliver Brunko for conducting the XRF analyses. The support of Beat Hornung, Marcel Rees, Anton Koster, and André Niederer are highly appreciated. The authors are very grateful to Steffen Ohr at Cham-Tenero Paper Mills Inc., Dr. Michael Plötze at ETH Zurich, and Dr. Philippe Tingaut for their useful advices and support, and we cordially thank Prof. Paul Smith for valuable discussions.

References

1. Bergaya F, Theng BKG, Lagaly G (eds) (2006) Handbook of clay science, vol 1
2. Murray HH (2007) Applied clay mineralogy: occurrences, processing, and application of kaolins, bentonites, palygorskite-sepiolite, and common clays. Elsevier, Boston
3. Chang J-H, Kim SJ, Joo YL, Im S (2004) Polymer 45(3):919
4. Yano K, Usuki A, Okada A (1997) J Polym Sci Part A 35(11):2289. doi:10.1002/(sici)1099-0518(199708)35:11<2289:aid-pola20>3.0.co;2-9
5. Mittal V (2008) J Compos Mater 42(26):2829
6. Brown G, Nadeau P (1984) Philos Trans R Soc Lond Ser A 311(1517):221. doi:10.1098/rsta.1984.0025
7. Jang SW, Kim JC, Chang JH (2009) Cellulose 16(3):445
8. Haydn HM (2000) Appl Clay Sci 17(5–6):207. doi:10.1016/s0169-1317(00)00016-8
9. Osman MA, Atallah A, Kahr G, Suter UW (2002) J Appl Polym Sci 83(10):2175
10. Subramaniyan AK, Sun CT (2006) Compos Part A 37(12):2257
11. Okamoto M, Morita S, Taguchi H, Kim YH, Kotaka T, Tateyama H (2000) Polymer 41(10):3887. doi:10.1016/s0032-3861(99)00655-2

12. Lee DC, Jang LW (1996) J Appl Polym Sci 61(7):1117–1122. doi:10.1002/(sici)1097-4628(19960815)61:7<1117::aid-app7>3.0.co;2-p
13. Lee YH, Park CB, Sain M, Kontopoulou M, Zheng W (2007) J Appl Polym Sci 105(4):1993
14. Fu X, Qutubuddin S (2000) Mater Lett 42(1–2):12. doi:10.1016/s0167-577x(99)00151-2
15. Sinha Ray S, Bousmina M (2005) Prog Mater Sci 50(8):962
16. Lilichenko N, Maksimov R, Zicans J, Merijs Meri R, Plume E (2008) Mech Compos Mater 44(1):45
17. Rhim J-W, Hong S-I, Ha C-S (2009) LWT Food Sci Technol 42(2):612
18. Rinaudo M, Lowys MP, Desbrières J (2000) Polymer 41(2):607. doi:10.1016/s0032-3861(99)00206-2
19. Azizi Samir MAS, Alloin F, Dufresne A (2005) Biomacromolecules 6(2):612. doi:10.1021/bm0493685
20. Bledzki AK, Gassan J (1999) Prog Polym Sci 24(2):221
21. Ho T, Zimmermann T, Hauert R, Caseri W (2011) Cellulose 18(6):1391. doi:10.1007/s10570-011-9591-2
22. Zimmermann T, Pöhler E, Geiger T (2004) Adv Eng Mater 6(9):754
23. Iwamoto S, Nakagaito AN, Yano H (2007) Appl Phys A 89(2):461
24. Paakko M, Ankerfors M, Kosonen H, Nykanen A, Ahola S, Osterberg M, Ruokolainen J, Laine J, Larsson PT, Ikkala O, Lindstrom T (2007) Biomacromolecules 8(6):1934. doi:10.1021/bm061215p
25. Hubbe MA, Rojas OJ, Lucia LA, Sain M (2008) BioResources 3(3):929
26. Siró I, Plackett D (2010) Microfibrillated cellulose and new nanocomposite materials: a review. Cellulose. doi:10.1007/s10570-010-9405-y
27. Eichhorn S, Dufresne A, Aranguren M, Marcovich N, Capadona J, Rowan S, Weder C, Thielemans W, Roman M, Renneckar S, Gindl W, Veigel S, Keckes J, Yano H, Abe K, Nogi M, Nakagaito A, Mangalam A, Simonsen J, Benight A, Bismarck A, Berglund L, Peijs T (2010) J Mater Sci 45(1):1. doi:10.1007/s10853-009-3874-0
28. Tingaut P, Zimmermann T, Lopez-Suevos F (2009) Biomacromolecules 11(2):454. doi:10.1021/bm901186u
29. Zimmermann T, Pöhler E, Schwaller P (2005) Adv Eng Mater 7(12):1156
30. Sehaqui H, Liu AD, Zhou Q, Berglund LA (2010) Biomacromolecules 11(9):2195. doi:10.1021/bm100490s
31. Liu A, Walther A, Ikkala O, Belova L, Berglund LA (2011) Biomacromolecules 12(3):633–641. doi:10.1021/bm101296z
32. Cerruti P, Ambrogi V, Postiglione A, Rychly J, Matisova-Rychla L, Carfagna C (2008) Biomacromolecules 9(11):3004. doi:10.1021/bm8002946
33. White LeslieA (2004) J Appl Polym Sci 92(4):2125
34. Zimmermann T, Bordeanu N, Strub E (2010) Carbohydr Polym 79(4):1086
35. Meier LP, Kahr G (1999) Anglais 47(3):386
36. Brindley GW, Brown G (1980) Crystal structures of clay minerals and their X-ray identification. Monograph no. 5, vol 495 S. Mineralogical Society, London
37. Mackenzie RC (1951) J Colloid Sci 6(3):219
38. Grim RE (1962) Applied clay mineralogy. McGraw-Hill, New York
39. Knödel K, Lange G, Voigt H-J, Altfelder S, Birke M, Dohrmann R, Hilse H, Jenn F, Kaufhold S, Nitsche C, Schmidt KR, Thiem A (2007) In: Environmental geology. Springer, Berlin/Heidelberg, pp 749–940. doi:10.1007/978-3-540-74671-3_17
40. Belbekhouche S, Bras J, Siqueira G, Chappey C, Lebrun L, Khelifi B, Marais S, Dufresne A (2011) Carbohydr Polym 83(4):1740. doi:10.1016/j.carbpol.2010.10.036
41. Favier V, Chanzy H, Cavaille JY (1995) Macromolecules 28(18):6365. doi:10.1021/ma00122a053
42. Abe K, Nakatsubo F, Yano H (2009) Compos Sci Technol 69(14):2434
43. Adame D, Beall GW (2009) Appl Clay Sci 42(3–4):545. doi:10.1016/j.clay.2008.03.005
44. Podsiadlo P, Kaushik AK, Arruda EM, Waas AM, Shim BS, Xu J, Nandivada H, Pumplin BG, Lahann J, Ramamoorthy A, Kotov NA (2007) Science 318(5847):80. doi:10.1126/science.1143176
45. Vertlib V, Dietiker M, Plötze M, Yezek L, Spolenak R, Puzrin AM (2008) J Mater Res 23(04):1026. doi:10.1557/jmr.2008.0147